NUCLEAR STRUCTURE -- THEORY

STRUCTURE OF THE COLLECTIVE LAGRANGIAN AND CLASSICAL LIMIT OF LIE ALGEBRAS

A. Bulgac and D. Kusnezov

A few years ago Berry[1] demonstrated the general significance of a phenomenon earlier studied in molecular structure,[2] now widely known as "Berry's phase". Mead[2] showed that in molecules, gauge fields can be generated dynamically and phenomena similar to the celebrated Aharonov-Bohm effect can be observed. Mead even coined the term Molecular Aharonov-Bohm effect for this class of new phenomena. Berry's work generated an explosion of scientific activity in almost every field in physics. So far in nuclear physics the only phenomenon exhibiting "Berry's phase" seems to be linked with the peculiar behavior of two neutron transfer amplitude in heavy ion reactions.[3] We have shown that Berry's phase can enter nuclear physics in a more fundamental way in collective motion. When constructing an effective Lagrangian/Hamiltonian for collective degrees of freedom, the noncollective degrees of freedom manifest themselves in part as dynamically generated gauge fields.[4] (Perhaps even genuine gauge fields may be generated this way.[5])

In Ref. 6 we showed how Berry's phenomenon appears in the case of time dependent HFB dynamics. We constructed the effective Lagrangian for the collective pairing degrees of freedom, which we subsequently requantized. To our knowledge, this is the first example where one explicitly (analytically) can requantize the ATDHFB Hamiltonian and show that the quantum solution can only be recovered after taking into account the dynamically generated gauge fields. This particular example led us to think that such a result must hold in general and gauge fields should be associated with any collective degrees of freedom, which indeed we proved in Ref. 7.

The real significance of the occurrence of gauge fields in the case of an effective Lagrangian/Hamiltonian for collective motion was revealed in the study of the classical limit of Lie algebras.[8] Lie algebras play a significant role in almost any aspect of the quantum description of the nature. The most common example is the algebra of spin operators. Other examples include different types of quantum collective models for nuclei, gauge theories of elementary particles, condensed matter physics and so on. Our goal here will be in recovering the classical limit for any (semisimple) Lie algebra. Classical trajectories play an enormous role at almost any level of quantum description. The wave functions are concentrated along the classical trajectories. Often, knowing the classical trajectories and the relatively small quantum fluctuations around them provides not only a simple but, most of the time, a very accurate picture.

In constructing the classical limit for a Lie algebra we shall follow a route opposite to that used to construct quantum objects from classical objects. The fundamental concept of classical mechanics is the phase space, i.e. the canonical coordinates and momenta, and the Poisson brackets. For a system with N degrees of freedom one needs N pairs of canonical coordinates and momenta, which satisfy the standard Poisson brackets

$$\{q_k,p_l\} = \delta_{kl},\{q_k,q_l\} = \{p_k,p_l\}=0, \qquad (1)$$

where k,l = 1, ..., N.

For any two functions, one can define the corresponding Poisson brackets as

$$\{F,G\} = \sum_{k=1}^{N} \left[\frac{\partial F}{\partial q_k}\frac{\partial G}{\partial p_k} - \frac{\partial F}{\partial p_k}\frac{\partial G}{\partial q_k}\right] . \qquad (2)$$

Given a Hamiltonian, the Hamilton equations of motions read

$$\frac{\partial q_k}{\partial t} = \frac{\partial H}{\partial p_k}, \quad \frac{\partial p_k}{\partial t} = -\frac{\partial H}{\partial q_k} \tag{3}$$

which can be derived from the variation of the classical action

$$S = \int [\sum_{k=1}^{N} p_k \dot{q}_k - H]dt. \tag{4}$$

In Feynman's formulation of the quantum mechanics the classical action S plays the central role. The functional integral representing Feynman's propagator is (we shall use $\hbar = 1$)

$$K = \int D[q]D[p] \exp\{-i \int [\sum_{k=1}^{N} p_k \dot{q}_k - H]dt\}. \tag{5}$$

The traditional route from classical to quantum mechanics consists in making the canonical variables operators and the Poisson brackets commutators and replacing the Kronecker's symbols by i times the corresponding Kronecker's symbols

$$[q_k,p_l] = i\delta_{kl}, [q_k,q_l] = [p_k,p_l] = 0, \tag{6}$$

where $k,l = 1,\ldots,N$.

The quantum equations of motion are obtained in a similar way.

An arbitrary Lie algebra is completely defined by the commutation relations among generators

$$[\hat{X}_j,\hat{X}_k] = ic_{jkl}\hat{X}_l, \tag{7}$$

where c_{jkl} are the structure constants. At the classical level we shall interpret the operators $\hat{X}_k$ as noncanonical variables on the classical phase space and define the symplectic structure through the following Lie-Poisson brackets

$$\{F,G\} = \sum_{jkl} \frac{\partial F}{\partial X_j} \frac{\partial G}{\partial X_k} X_l c_{jkl}, \tag{8}$$

where F,G are some arbitrary functions of X_k. Our task consists now in identifying the canonical variables as functions of the classical quantities X_k and the construction of the classical action corresponding to a given Lie algebra. Once this is done the requantization procedure will be more or less straightforward, either at the level of Bohr-Sommerfeld rules or in the framework of Feynman's functional integral approach. Even though this program seems to be relatively well defined, there are a number of subtleties, due mainly to the unusual topology of the classical phase space, which are crucial in reaching a correct description both at the classical level and subsequently in the requantization procedure. We shall exemplify our construction only for the case of SU(2). The SU(2) Lie-Poisson bracket is then

$$\{F,G\} = \sum_{jkl} \epsilon_{jkl} \frac{\partial F}{\partial J_j} \frac{\partial G}{\partial J_k} J_l = \nabla F \times \nabla G \cdot J, \tag{9}$$

where F,G are any two functions of J_x,J_y and J_z. A remarkable property of this Lie-Poisson bracket is that for an arbitrary function $H(J_x, J_y, J_z)$, $\{H, J_x^2+J_y^2+J_z^2\} \equiv 0$. When H is the Hamiltonian of a rigid top one recovers the Euler equations from

$$\frac{\partial J}{\partial t} = \{J,H\} = \nabla H \times J.$$

Due to the special form of the SU(2) Lie-Poisson bracket, the classical trajectories of any Hamiltonian will always be confined to the 2-sphere S_2. Consequently, the space of all possible states will always be compact. It is obvious that in this case one can have at most one coordinate and one momentum only. Consider the SU(2) Poisson brackets of the generators in a neighborhood of the North pole

$$\{\frac{J_x}{\sqrt{J_z}}, \frac{J_y}{\sqrt{J_z}}\} = 1 + \frac{J_x^2}{2J_z^2} + \frac{J_y^2}{2J_z^2} = 1 + o(\varepsilon^2),$$

$$\{\frac{J_x}{\sqrt{J_z}}, J_z\} = -\frac{J_y}{\sqrt{J_z}} = o(\varepsilon), \quad \{\frac{J_y}{\sqrt{J_z}}, J_z\} = \frac{J_x}{\sqrt{J_z}} = o(\varepsilon). \tag{10}$$

These Poison brackets assume an almost canonical form near the North pole, where $J_x \sim J_y \sim o(\varepsilon)$, where ε is arbitrarily small. Thus, near the North pole the first Poisson bracket is $1+o(\varepsilon^2)$, and the remaining brackets are $o(\varepsilon)$. At the point $J_x=J_y=0$ one can identify $q = J_x/\sqrt{J_z}$ and $p = J_y/\sqrt{J_z}$. Since the North pole is an arbitrary point on the sphere, one can use these local canonical coordinates in order to define globally the symplectic 2-form

$$\omega = dp \wedge dq = \frac{J_z dJ_x \wedge dJ_y + J_y dJ_z \wedge dJ_x + J_x dJ_y \wedge dJ_z}{J_x^2+J_y^2+J_z^2} \tag{11}$$

It can be shown that

$$\omega = \sqrt{J_x^2+J_y^2+J_z^2}\, dA, \quad A = \frac{J_z(J_y dJ_x - J_x dJ_y)}{(J_x^2+J_y^2)\sqrt{J_x^2+J_y^2+J_z^2}}, \tag{12}$$

where the "gauge" potential A describes a Dirac monopole located at the origin. The classical action for SU(2) is therefore

$$S = \int [\sqrt{J_x^2+J_y^2+J_z^2}\, A - H dt], \tag{13}$$

where the integral is along the trajectory. If the trajectory is closed, one can use the Stokes theorem and transform the loop integral into a surface integral,

$$S = \oint [\sqrt{J_x^2+J_y^2+J_z^2}\, A - H dt] = \int\int_{A_{1,2}} [\omega - dH \wedge dt], \tag{14}$$

where $A_{1,2}$ represent the two possible choices of the surface enclosed by the closed (periodic) trajectory. When used in a path integral formulation of the quantum theory, the two different choices of the surfaces must lead to results which differ by an integer number of 2π, since the classical action appears as a phase. This amounts to the the following restriction upon the allowed spheres at the quantum level

$$\int\int_{S_2} \omega = 4\pi\sqrt{J_x^2+J_y^2+J_z^2} = 2\pi n, \tag{15}$$

which is the quantization of the total angular momentum, which can be only half-integer or integer, depending on the radius of the S_2 sphere. Besides the total spin, the Bohr-Sommerfeld quantization rule $\oint pdq \equiv \oint A = 2\pi n$ fixes the projection of the spin on an arbitrary axis with values $-J,\ldots,J$. One can define in a completely analogous way the classical limit for any Lie algebra. For higher rank algebras, the topology of the classical phase space is more complicated, due to the appearance of a larger number of constraints (Casimirs) on the generators. The number of "gauge" potentials arising in this way is larger, and the quantization rules more complicated. However, the general features are very similar to the case of SU(2). An extensive discussion and references can be found in Ref. 8.

The nuclear many-body problem can be formulated in the language of a Lie algebra. Pairs of creation and annihilation operators generate either the orthogonal SO(2N) or unitary SU(N) algebra, where N is the dimension of the single-particle Hilbert space. In a (time-dependent) mean field treatment these pairs of operators are replaced by their mean value, which is a c-number and therefore one is dealing with a classical limit of a quantum theory. The classical phase space is realized by replacing the Lie algebra generators with c-numbers and by introducing the appropriate symplectic structure. One feature of the quantum version of a Lie algebra survives in the classical limit: the conservation of Casimirs operators. This makes the topology of allowed

trajectories nontrivial and the formalism is similar to Dirac's constrained dynamics. The phase space splits into (symplectic) leaves of nontrivial shapes and the necessity of introducing a connection is obvious. The curved nature of the phase space and the nontrivial topology of the trajectories make the requantization procedure highly nontrivial. The modified Poisson structure of the collective phase space was also remarked recently in Ref. 9. We should mention that a classical limit for Lie algebras can be defined by starting from a coherent state approach.[10] There are certain conceptual differences between the two approaches and in our opinion, the direction followed in Refs. 8 and 9 is better suited and more natural for the purposes of large amplitude collective motion.

References

1. M.V. Berry, Proc. Roy. Soc. London, Ser.A 392,45(1984).
2. C.A. Mead , D.G. Truhlar, J. Chem. Phys. 70,2284(1979); C.A. Mead, Chem. Phys. 49, 23 and 33(1980), J. Chem. Phys. 72,3839 (1980), 78,307(1980), Phys. Rev. Lett. 59,161(1987); S.P. Keating, C.A.Mead, J. Chem. Phys. 82,5102(1985), 86,2152(1987); T.C. Thompson, C.A. Mead, J. Chem. Phys. 82,2408 (1985).
3. R.S. Nikam and P. Ring, Phys. Rev. Lett. 58,980(1987).
4. A. Bulgac, Phys. Rev. A37,4048(1988).
5. F. Wiczek and A. Zee, Phys. Rev. Lett. 52, 2111(1984).
6. A. Bulgac, Phys. Rev. C41,(1990) (in press).
7. A. Bulgac, Phys. Rev. C40,2840(1989).
8. A. Bulgac and D. Kusnezov, Ann.Phys. 199, 225(1990).
9. R. Balian and M. Veneroni, Ann.Phys. 195, 324(1989).
10. R.L. Klauder and Skagerstam, Coherent States, World Scientific, 1985; R. Gilmore, Ann. Phys. 74,391(1972), Rev. Mex. de Fisica 23,142(1974); A.M.Perelomov Commun. Math. Phys. 26,222(1972).

CROSS-SHELL EXCITATIONS AROUND ^{32}Mg

B. Alex Brown, E. K. Warburton[a] and J. A. Becker[b]

The anomalies in the binding energies, excitation energies, half-lives and radii of the most neutron rich Na and Mg isotopes relative to 0$\hbar\omega$ shell-model calculations have been known for a long time.[1] The situation has been referred to as the "collapse of the conventional shell model".[2] Several studies over the past ten years have indicated that the problem is due to low-lying intruder states from the pf shell.[3,4,5] We have carried out new systematic calculations with the W-MG-WBMB interaction for these intruder states.[6] These new calculations incorporate all of the sd and pf orbits and represent the most ambitious calculations to date. An advantage (and disadvantage) of our calculations is that there are no adjustable parameters. The W-sd and MG-pf parts of the interactions were already well established. The WBMB cross-shell interaction[7] was obtained from a fit of the Millener-Kurath potential model[8] parameters and some fine tuning of some individual two-body matrix to reproduce the excitation energies of 1p-1h states in ^{40}Ca and ^{40}K.

An important aspect of our calculations is that we do not allow for explicit mixing between 0$\hbar\omega$, 2$\hbar\omega$, 4$\hbar\omega$, etc. configurations or between 1$\hbar\omega$, 3$\hbar\omega$ etc. configurations. The rationale for this restriction is related to the "excitation-order" problem discussed in Ref. 9 and is discussed more in the present context in Ref. 6. The standard shell-model interactions we are familiar with, such as the W-sd interaction, are designed to reproduce binding energies without such explicit mixing and must already incorporate this mixing implicitly. Our experience with the well-known n$\hbar\omega$ intruder states near ^{16}O and ^{40}Ca indicates that these different excitations tend to "coexist" rather than to strongly mix with each other. Our point of view is that we do not at present know how to deal with explicit mixing and that hopefully "coexistence" will continue to hold.

This is one of the major differences between our calculations and those of Poves and Retamosa where explicit mixing between major shells is allowed. Poves and Retamosa mix an extremely deformed 2$\hbar\omega$ ground state band (e.g. with the 2^+ energy around 200 keV) with the normal 0$\hbar\omega$ states to get resulting spectra which are moderately deformed (e.g. with the 2^+ energy around 800 keV). Our calculation, with no mixing, and the Poves-Retamosa calculation, with large mixing, give qualitatively the same spectra in cases where the experimental data were known before the calculation. We will point out at the end of this section several places where important differences between the calculations are expected which could be tested experimentally.

To study the intruder states we carried out calculations where one or two nucleons were allowed to be excited from the sd to the pf shell. Many of the calculations could be carried out in the full sd-pf space. However there were also many cases of interest around ^{32}Mg which had dimensions which are too large (>10,000) to handle. We investigated several truncations which have promise for future calculations. However, the most interesting and useful result found in these investigations is that a weak-coupling model can be used to relate the excitation energy of the n$\hbar\omega$ configurations to the calculated 0$\hbar\omega$ binding energies in nuclei with neighboring neutron numbers. Details of the weak coupling model are given in Ref 6.

For nuclei around ^{32}Mg we find an "island of inversion" where 1$\hbar\omega$ and 2$\hbar\omega$ neutron excitations from the sd to the pf shell lie lower in energy than the normal "0$\hbar\omega$"

configuration. We found that there are three mechanisms which combine to give this inversion: a small reduction in the effective single-particle energy gap, the pairing energy E_{nn}, and the proton-neutron interaction energy E_{pn}. The only one of which should have a strong Z dependence is E_{pn}.

In Ref. 6 we discuss many examples where the qualitative aspects of our weak-coupling calculations agree with experiment. Here we give a few examples and some comments on places where more experimental data are needed and/or where more calculations are needed.

(a) The low excitation energy of both the $1\hbar\omega$ (Fig. 5 in Ref. 6) and $2\hbar\omega$ (Fig. 4 in Ref. 6) configurations in ^{31}Mg are consistent with the recent data which shows a large level density at low excitation energy.[10] However, we are not able at present to calculate the precise order of these configurations or the order of the states within a given configuration. We note that ^{31}Al has experimental β decay properties as well as low-lying levels which agree with the the sd calculation, but that ^{31}Mg has experimental β decay properties which are in complete disagreement with the sd calculation.[11] This indicates that the ground state of ^{31}Mg is not the expected $3/2^+$ sd configuration, but is a $1\hbar\omega$ or $2\hbar\omega$ configuration. More experiments and calculations are needed to sort out the possibilities.

(b) In ^{34}Si, the 2^+ state seen experimentally at 3.33 MeV is close to where we would expect our 2^+ $2\hbar\omega$ state. The negative parity states near 4.3 MeV are close to where we predict the $1\hbar\omega$ excitations to start (see Fig. 5 in Ref. 6) and are also consistent with the β decay of ^{34}Al.[12] The Poves-Retamosa calculations are also in reasonable agreement for these known states.[13] However, we predict a 0^+ state from the $2\hbar\omega$ configuration around 1.5 MeV (see Fig. 4 in Ref. 6), whereas the Poves-Retamosa calculation puts this excited 0^+ state near 4 MeV. This state has not yet been observed experimentally.

(c) In ^{32}Mg the known 2^+ state at 0.88 MeV is close to where we expect the first excited state of the $2\hbar\omega$ ground-state band. Because the $1\hbar\omega$ and $2\hbar\omega$ configurations in ^{32}Na are close in energy (and both below the $0\hbar\omega$ configuration) the states around 3.0 MeV in ^{32}Mg seen in the ^{32}Na β decay have several interpretations in our model. If ^{32}Na has a $2\hbar\omega$ ground state then it would have a negative parity and would decay to the negative-parity states expected around 3 MeV in ^{32}Mg. If ^{32}Na has a $1\hbar\omega$ ground state we predict that this would be 0^+ and then it would decay to 1^+ states in ^{32}Mg which could also lie around 3 MeV (we have not yet made calculations for these 1^+ states). The excitation energy in ^{32}Mg of our predicted 0^+ state from the $0\hbar\omega$ configuration is around 1 MeV (see Fig. 4 in Ref. 6). In contrast, the Poves-Retamosa calculations predict a 4^+ state at about this excitation energy. More experimental information is needed to test these predictions.

(d) The most serious disagreement with our present calculations is the underbinding of ^{32}Na and ^{33}Na. Even though our intruder states come below the $0\hbar\omega$ configurations for these nuclei, it is not enough to explain the magnitude of the discrepancy indicated in Fig. 2 of Ref. 6. It would be very useful to have new experimental data for the masses of the neutron rich Ne and Na isotopes. Continued disagreement with experiment may indicate, for example, that our extrapolated pf single-particle energies are incorrect.

(e) For the secondary-beam experiments which may eventually be possible, we would like to suggest that one-nucleon transfer experiments will provide the most valuable spectroscopic information for improving the calculations. Theoretical extrapolations of the single-particle energies in nuclei far from stability are difficult and uncertain. They are also the most important single ingredient for the understanding of more detailed aspects of the structure.

(f) Calculations are needed for the β-decay

properties of the intruder states. In particular, the unusual half-life and decay properties of ^{31}Mg (Ref.11) must be understood.

---

a. Brookhaven National Laboratory, Upton, New York 11973.
b. Lawrence Livermore National Laboratory, Livermore, CA 94550

References

1. C. Thibault et al., Phys. Rev. C12,644 (1975); C. Detraz et al., Nucl. Phys. A394, 378(1983); C. Detraz et al., Phys. Rev. C19,164(1979).
2. B. H. Wildenthal and W. Chung, Phys. Rev. C19,164(1979).
3. X. Campi et al., Nucl. Phys. A251,193 (1975).
4. A. Poves and J. Retamosa, Phys. Lett. B184 311(1987).
5. M. H. Storm, A. Watt and R. R. Whitehead, J. Phys. G9,L165(1983); A. Watt, R. P. Singhal, M. H. Storm and R. R. Whitehead, J. Phys. G7,L145(1981).
6. E. K. Warburton, J. A. Becker and B. A. Brown, Phys. Rev. C41,1147(1990).
7. E. K. Warburton, J. A. Becker, D. J. Millener and B. A. Brown, BNL Report 40890 (1987).
8. D. J. Millener and D. Kurath, Nucl. Phys. A255,315 1975).
9. B. A. Brown and B. H. Wildenthal, Ann. Rev. of Nucl. and Part. Sci. 38,29(1988).
10. P. Baumann et al., unpublished.
11. B. H. Wildenthal, M. S. Curtin and B. A. Brown, Phys. Rev. C28,1343 (1983).
12. E. K. Warburton and J. A. Becker, Phys. Rev. C37,754(1988).
13. P. Baumann et al., Phys. Lett. 228B,458 (1989).

BINDING ENERGIES FOR NEUTRON-RICH NUCLEI

B. Alex Brown

There has been excitement recently about the apparent instability of ^{26}O.[1] We show in Fig. 1 binding energy curves for the O isotopes. The experimental data are compared with three predictions: the global predictions of Moeller and Nix,[2] the W-sd calculation up to N=20[3] plus the W-MG-WBMB-sd-pf calculation beyond N=20[4] and the SDPOTA-sd calculation[5] up to N=20. For the established data, the shell-model predictions are clearly much better than the global-model

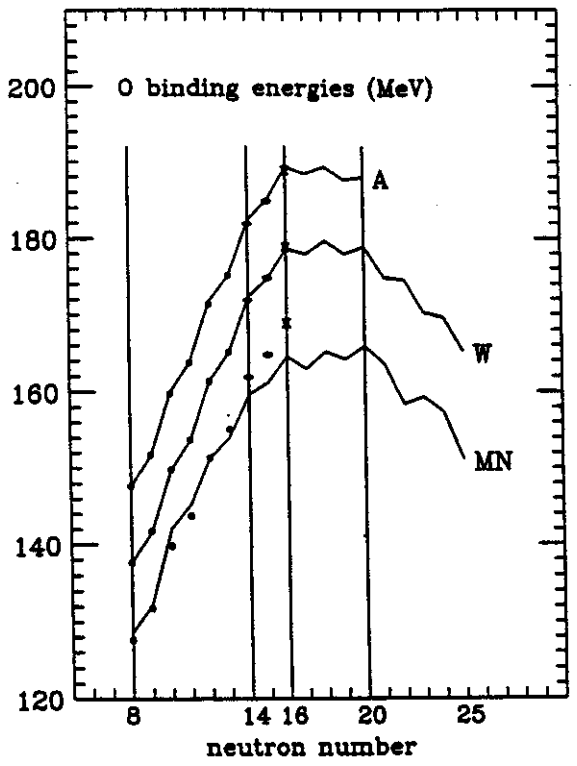

Fig. 1 Binding energies of the ground states of the oxygen isotopes. (a) The experimental energies (solid circles) are compared to three calculations (solid lines) discussed in the text: Moeller-Nix (MN), W-sd for $N \leq 20$ plus W-MG-WBMB-sd-pf for $N \geq 20$ (W), and SDPOTA-sd (A). For display 10 MeV has been added to the W comparison and 20 MeV has been added to the A comparison.

predictions in this case. The average deviation between the shell-model predictions and experiment is consistent with the average 180 keV rms deviation found for 447 ground and excited states over the entire sd shell.[3,6] The global model of Moeller and Nix, as well as most other global models,[7] predict that ^{26}O is stable in contradiction to experiment. However, this is not too surprising, given the rather poor agreement for the other oxygen isotopes. It is more surprising that the W-sd calculations also predicts that ^{26}O is stable by about 1 MeV. However, the SDPOTA-sd calculation predicts ^{26}O to be unstable, but only by 20 keV! This difference is an indication of the rather large model dependence which can exist in the shell-model extrapolations to exotic nuclei. With both W and SDPOTA ^{27}O and ^{28}O are predicted to be unstable.

The trend of the oxygen binding energies can be understood in the extreme j-j coupling limit. We show in Fig. 2 the effective neutron single-particle energy (ESPE) as a function of neutron number in this j-j coupling limit. The neutron ESPE are seen to be rather constant as a function of neutron number. This leads to a simple qualitative interpretation for the binding energy curve shown in Fig. 1. Between N=8 and 14 the neutrons fill the $d_{5/2}$ orbit which is bound in ^{16}O by about 4 MeV. This, together with the attractive pairing energy, provides the sharp increase in binding energy observed between N=8 and 14. Between N=14 and 16 the neutrons fill the $s_{1/2}$ orbit which is less bound than the $d_{5/2}$. Thus one starts to see less increase in the binding energy at this point. Between N=16 and 20 the neutrons fill the $d_{3/2}$ orbit which has close to zero energy, and the binding energy curve becomes flat in this region. This flatness, of course, makes it difficult to predict exactly which nuclei will be stable, which is what makes this region so

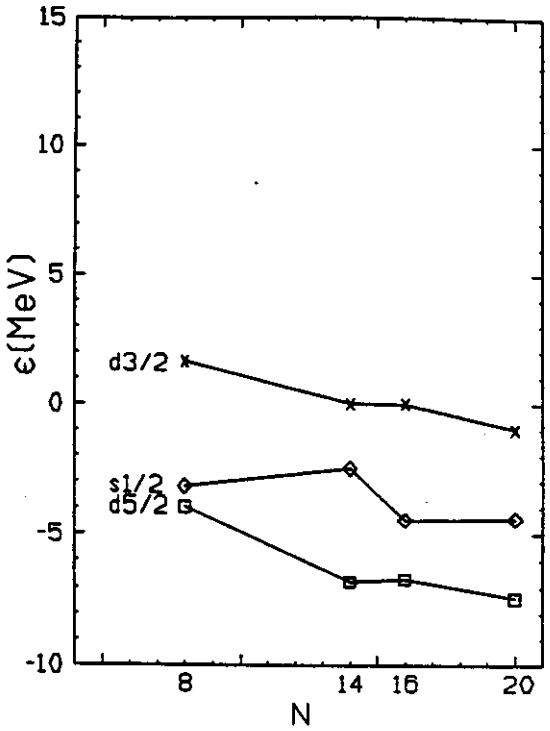

Fig. 2 Neutron single-particle energies for the oxygen isotopes (Z=8) as a function of neutron number. The values at N=14 and 16 were obtained in the extreme j-j coupling limit.

interesting from the stability point of view. Beyond N=20 the neutrons must start to go into the pf shell orbits which are unbound. Hence the binding energy curve decreases beyond this point. This marks the end of where the oxygen isotopes can be studied and also the end of where they need to be understood for astrophysical purposes.

At the next level of detail we should take into account the small shifts in the neutron ESPE shown in Fig. 2. These are due to the interactions within the shells. For example the shift in the $s_{1/2}$ ESPE between ^{16}O and ^{22}O is due the monopole average over two-body matrix elements:

$$\Sigma_J(2J+1)\langle d_{5/2},s_{1/2},J|V|d_{5/2},s_{1/2},J\rangle/\Sigma_J(2J+1)$$

It is important to note that these two-body matrix elements can in principle be obtained from information on excited states in ^{18}O and ^{19}O etc. Data on excitation energies relevant to these $d_{5/2}$-$s_{1/2}$ two-body matrix elements were included in the 447 fit-data set used to obtain the W and SDPOTA interactions. Hence, the good agreement for the ^{23}O and ^{24}O mass predictions may not be surprising even though data on these two nuclei were not included in the fit-data set. In contrast, beyond ^{24}O, the ESPE depend on the $d_{5/2}$-$d_{3/2}$ two-body matrix elements. Data on excitation energies relevant to these do not exist because they are more highly excited configurations and lie in a large level density of intruder states. Hence beyond ^{24}O, the predictions rely more on assumptions in the calculation which cannot be tested from previously known data. For the W interaction this is the Kuo-Brown G matrix used for the poorly determined linear combinations, and for the SDPOTA interaction this is the particular form of the potential model assumed (a modified surface one-boson exchange potential).

The actual sd-shell calculations shown in Fig. 1 go beyond j-j coupling and include all possible sd-shell configurations, but the dominant configurations are those assumed above. These calculations, it should be remembered, are based on an assumed constancy of the bare SPE and an assumed simple $(A/18)^{0.3}$ mass dependence of the two-body matrix elements.[3,6]

In contrast to the relative constancy of the neutron ESPE as a function of neutron number, they quickly decrease as a function of proton number. By the time one reaches ^{40}Ca all of the sd-shell orbits as well as the pf-shell orbits are bound. At N=20 the ESPE of the neutron orbits as a function of N should again be relatively constant, and applying the same qualitative argument as above, we can see that all Ca isotopes out to ^{60}Ca should be stable. The stability in the region between ^{60}Ca and ^{70}Ca depends on exactly what the value of the ESPE for the $g_{9/2}$ orbit is at this point.

Binding-energy comparisons have been made for Z=9-20 similar to the ones shown in Fig. 1 for Z=8. We show the differences between

experiment and the theoretical predictions in Fig. 3. The predictions are based on W-sd for N $\leq$ 20 and W-MG-WBMB-sd-pf for N > 20. New data on the F and Ne isotopes have been included.[8] We first discuss the stability properties which are not shown in Fig. 3. ^{28}F is predicted to be

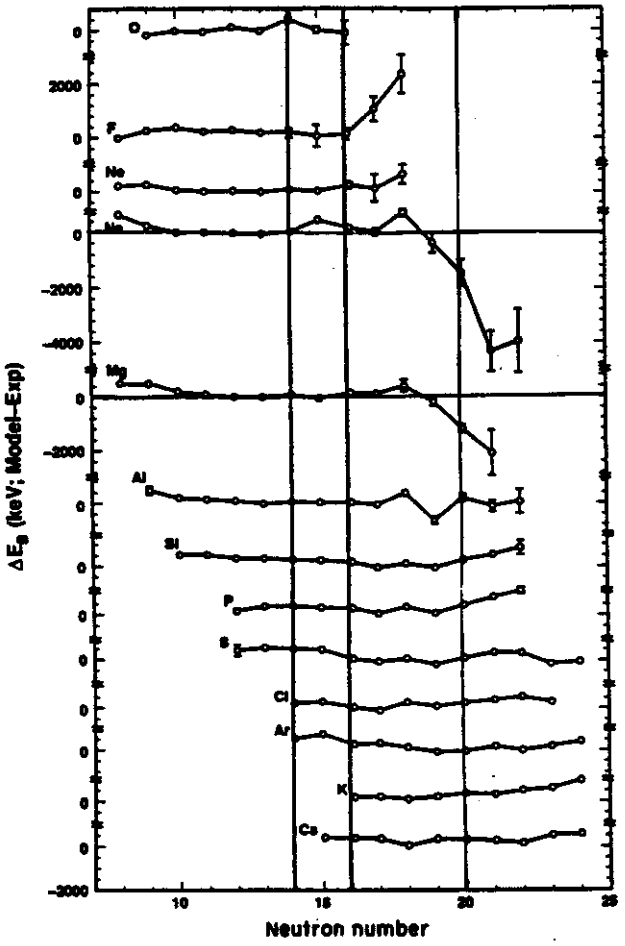

Fig. 3 Difference between the measured and calculated binding energies for the sd and sd-pf regions.* The calculation is W-sd for N $\leq$ 20 and W-MG-WBMB-sd-pf for N $\geq$ 20. The lines indicate the semi-magic numbers N=14 and 16 and the zero for the Na and Mg isotope differences.

unstable and ^{29}F is predicted to be stable by both W and SDPOTA in agreement with experiment.[1] W-MG-WBMB predicts all F nuclei to be unstable beyond this point. ^{29}Ne is predicted to be unstable by 129 keV with the W interaction and by 4 keV with the SDPOTA interaction. Hence the disagreement with experiment[1] is not too surprising. ^{30}Ne and ^{32}Ne are predicted to be stable and ^{31}Ne unstable in agreement with experiment. Beyond these only ^{34}Ne is predicted to be stable. All remaining nuclei in the sd-shell (N $\leq$ 20) for Z > 10 are predicted to be stable, in agreement with experiment. And for N > 20 and Z > 10 the W-MG-WBMB calculations have not yet been carried out far enough in neutron number to predict where the drip line is.

The differences shown in Fig. 3 show excellent agreement between experiment and theory for most cases. We emphasize that the shell-model is a successful model for excitation energies as well as ground state masses.[3,6] There are a few exceptional deviations in Fig. 3. For N=18 and 9 $\leq$ Z $\leq$ 13 there is an obvious glitch which may be due to a similar kind of model-dependence left in the W interaction as discussed above for ^{26}O. The more dramatic deviations in the most neutron rich Na and Mg isotopes, which have been known for many years,[9] point to the intruder state problem.[4] The next major step in the sd-shell calculations will be to incorporate all of the new data which has appeared since the original fit-data set was put together about ten years ago.

References

1. D. Guillemaud-Mueller et al., Phys. Rev. C41,937(1990).
2. P. Moeller and J. J. Nix, At. Data Nucl. Data Tables 39,231(1988).
3. B. H. Wildenthal, Progress in Particle and Nuclear Physics 11, edited by D. H. Wilkinson (Pergamon, Oxford, 1984) p. 5.
4. E. K. Warburton, J. A. Becker and B. A. Brown, Phys. Rev. C41,1147(1990).
5. B. A. Brown, W. A. Richter, R. E. Julies and B. H. Wildenthal, Ann. Phys. 182,191(1988).
6. B. A. Brown and B. H. Wildenthal, Ann. Rev. of Nucl. and Part. Sci. 38,29(1988).
7. A. H. Wapstra, G. Audi and R. Hoekstra, At. Data Nucl. Data Tables 39,281(1988).
8. D. J. Vieira et al., Phys. Rev. Lett. 57, 3253(1986); A. Gillibert et al., Phys. Lett. 192B,39(1987).
9. C. Thibault et al., Phys. Rev. C12, 644 (1975); C. Detraz et al., Nucl. Phys. A394, 378 (1983); C. Detraz et al., Phys. Rev. C19, 164 (1979).

ADIABATIC TIME-DEPENDENT HARTREE-FOCK THEORY AND GENERALIZED VALLEY APPROXIMATION

A. Bulgac, A. Klein,[a] N. Walet[a] and G. Do Dang[b]

In recent years we have been working on the development and application of a constructive method for studying adiabatic large-amplitude collective motion (LACM).[1-7] During the last 20 years many important contributions have been made to the subject (see references cited in Refs. 1-7). Our constructive procedure for determining the collective subspace starts from a time-dependent Hartree-Fock (TDHF) description. Even though this looks like a quantum description, it is well known that in a certain sense the TDHF equations are classical in nature and can be written as such, i.e. in an explicit Hamiltonian form, with well defined canonical coordinates and momenta. Consequently, the search for collective modes can thus be viewed as a problem in classical mechanics; one searches for decoupled motions of the system, expecting that the slow and fast degrees of freedom will display vastly different evolution time scales. In an ideal situation these degrees of freedom will be completely independent.

The cornerstone of our approach to this problem, which we have named the Generalized Valley Approximation (GVA), is a theorem in classical mechanics, which we have proved. The theorem allows one to characterize the collective manifold in such a way as to actually construct it, by solving a certain overcomplete set of equations (i.e. the number of equations to be satisfied is much larger than the dimensionality of the collective subspace). In the ideal case, when an exactly decoupled collective subspace exists, all these equations are exactly satisfied. In particular, the method of separation of coordinates can be derived as a special solution of these equations. In cases of practical interest, the slow and fast degrees of freedom are never exactly decoupled and consequently, rigorously they can never be strictly defined. In mathematical terms this situation is reflected in the fact that there is no solution to the overcomplete (infinite) set of equations we derive, using the above mentioned theorem. The way out of this seemingly contradictory situation is a "physical" approach. One solves exactly only a finite number of these equations (equal to the dimension of the sought after collective subspace) and the degree of nonexactness of the remaining ones serves as a measure of our decoupling procedure. Fortunately, one can characterize in rather simple physical terms the reasons why one is not able to exactly decouple the collective degrees of freedom from the noncollective ones. One reason is linked with the appearance of centrifugal forces, another is real forces acting orthogonal to the collective subspace. In the case one achieves an approximate decoupling, these forces are rather small. By always checking the validity of the decoupling procedure one can determine in principle the optimal dimension of the collective subspace. The procedure is rather simple, one starts with decoupling one collective coordinate, if the criteria for the validity of the decoupling are not met one includes one more dimension in the collective set, and so on. Even though the criteria for the validity of the decoupling are not satisfied at the required level, the collective subspace so determined is still a part of the larger one, so the work done does not go down the tube.

When translated back to usual formulation of the ATDHF theory, our procedure of decoupling a collective subspace looks formally like a cranking method, where the number of cranking operators is equal to the number of collective degrees of freedom. The only difference is in

the way one should compute the cranking operators along the collective path or submanifold. The cranking operators change along the path in a prescribed way if one wants to minimize the coupling to the noncollective degrees of freedom.

One more advance we have achieved in our treatment consists of substantially enlarging the class of allowed cranking operators, while still developing an adiabatic theory. In the traditional approaches to this problem, including our older one, the cranking operator was a functional of only time-even Slater determinants along the path, which play the role of coordinates. In the study of a soluble model of monopole vibrations, we showed however that such an approach is not able to produce the right result (in particular the collective mass). The cranking operator has a more complicated structure as expected; and in the class of considered candidates one should include cranking operators depending on both time-even and time-odd Slater determinants, or in other words, the class of allowed canonical transformations from the initial set of coordinates to the new ones (decoupled) should be larger than simply point transformations.

The methods developed by us are going to be useful for other problems as well, such as chemistry, solitons, quantization of non-separable systems and so on.

---

a. University of Pennsylvania, Philadelphia, PA 19104.
b. Laboratoire de Physique Theorique et Hautes Energies, Univ. de Paris Sud, 91405 Orsay, France.

References

1. G. Do Dang, A. Bulgac, A. Klein, Phys. Rev. C36,2661,(1987).
2. A. Bulgac, A. Klein, G. Do Dang , Phys. Rev. C36,2672(1987).
3. A. Bulgac, A. Klein, G. Do Dang, Phys. Lett. B191,217(1987).
4. A. Bulgac, A. Klein, G. Do Dang, Nucl. Phys. A490,275(1988).
5. A. Bulgac, A. Klein, G. Do Dang, Phys. Rev. C37,2156(1988).
6. A. Bulgac, A. Klein, N.R. Walet and G.Do Dang, Phys. Rev C40,945(1989).
7. N.R. Walet, A. Klein, A. Bulgac and G. Do Dang, Phys. Rev. C41,318(1990).

TWO-NEUTRINO DOUBLE BETA DECAY OF ^{48}Ca

L. Zhao, B. A. Brown, and W. Richter[a]

Double beta ($\beta\beta$) decay is a rare transition between two nuclei of the same mass number having a change of two units of nuclear charge. In cases of interest, ordinary single beta decay is forbidden because of the energy conservation or angular momentum mismatch. There are two modes of double beta decay, one involving the emission of two antineutrinos and two electrons (2ν mode), it occurs in second order of the standard weak interaction theory and is independent of a possible small neutrino mass. The other involving no neutrinos and two electrons (0ν mode), violates the lepton number conservation and requires the neutrino to have a nonzero mass.[1,2,3] Analysis of the experimental result to determine the character of the neutrino in $\beta\beta$ decay strongly depends on the precise calculation of the nuclear matrix elements. In particular, agreement between the experiment and theory for the standard 2ν mode is one of the prerequisites for a reliable interpretation of the more exotic 0ν mode. In this paper, we study the $2\nu\beta\beta$ of ^{48}Ca which has the largest double beta decay Q-value of any nucleus.

We have calculated the nuclear matrix elements for $2\nu\beta\beta$ decay of ^{48}Ca and the related β^- and β^+ decay in the $0f_{7/2}$, $1p_{3/2}$, $0f_{5/2}$, $1p_{1/2}$ (fp) shell-model space with a much larger basis than previously used and with a new and more reliable effective interaction than previously used. The truncation in the fp shell is defined by the set of partitions $f_{7/2}^{8-n}(p_{3/2}, f_{5/2}, p_{1/2})^n$. In this work, the partitions assumed for ^{48}Ca(0^+,T=4), ^{48}Sc(1^+,T=3) and ^{48}Ti(0^+,T=2) are ($n\leq 4$), ($n\leq 5$) and ($n\leq 4$), respectively. The $n\leq n_{max}$ means that n=0, ..., n_{max} are allowed. The corresponding J-scheme dimensions are 133, 5599 and 3613, respectively. Our calculations were carried out with the shell-model code OXBASH[8] on a VAX computer.

The effective interactions used in are called MH[9] and MSOBEP.[10] The MH interaction has a long history.[9,11,12,13] MSOBEP is a new effective interaction based on a modified surface (MS) one-boson exchange potential (OBEP).[14] Modified refers to the addition of monopole (infinitely long range) terms to the central part of the potential, and surface refers to an assumed density dependence which empirically is surface peaked. This MSOBEP potential has been successful in reproducing the sd-shell energy levels in terms of a few parameters associated with the strengths of the various OBEP channels. Richter et al.[10] have recently refit the parameters of this potential to 61 energy level data in the lower part of the fp shell, and this is the new interaction which we employ in the present work.

Based on previous beta decay and (p,n) reaction studies,[15] we use the effective Gamow-Teller operator

$$\tilde{\sigma} = \frac{g_A^{eff}}{g_A}\,\sigma = 0.77\sigma \qquad (1)$$

For purposes of discussion, we introduce the matrix element for the $2\nu\beta\beta$ decay,

$$M_{GT}(E_m) = \sum_{m=1}^{E_m} M_{GT}^m$$

$$= \sum_{m=1}^{E_m} \frac{\langle 0_f^+||\tilde{\sigma}t^-||1_m^+\rangle\langle 1_m^+||\tilde{\sigma}t^-||0_i^+\rangle}{E_m + E_0} \qquad (2)$$

which is a function of the 1^+ excitation energy E_m in ^{48}Sc. $E_0 = T_0/2 + \Delta M$, where T_0 is the Q-value for $\beta\beta$ decay of ^{48}Ca and ΔM is the mass difference between ^{48}Sc and ^{48}Ca, T_0=4.27 MeV and ΔM=-0.277 MeV.[21] The total matrix element

for $2\nu\beta\beta$ is given by $M^{2\nu}_{GT}=M_{GT}(E_m = \infty)$. The Fermi transition contribution vanishes when isospin is conserved. An estimate of its contribution with isospin-mixed wave functions indicates that it is small and can be neglected.[1] The half life is given by

$$\frac{1}{T_{1/2}} = G|M^{2\nu}_{GT}|^2 \qquad (3)$$

where G is related to fundamental constants and the phase space integral.[3] In fact, G depends somewhat on the GT strength distribution[3,4] as well. Since the strength distribution of Ref. 4 is close to ours, we use a value of $G=1.10 \times 10^{-17}$ $yr^{-1}(MeV)^2$ deduced from the first row in Table 1 of Ref. 4.

The calculated matrix elements $M_{GT}(E_m)$ as a function of E_m for the MH and MSOBEP interactions are shown in Fig. 1. There are about 300

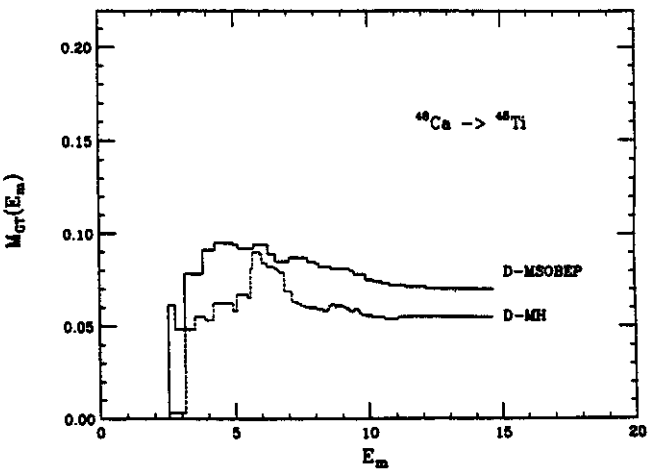

Fig. 1 $M_{GT}(E_m)$ as a function of E_m. The first $M_{GT}(E_m)$ is fixed at E_1=2.52 MeV. The solid line is obtained from the MSOBEP interaction, and dashed line from the MH interaction.

eigenstates in each curve from 2.52 MeV - 15 MeV. The $M^m_{GT}(E_m)$ become negligibly small after about 12 MeV even though there are still many 1^+ states (over 5000) above this energy in the calculation.

To understand the $\beta\beta$ matrix elements, we examine the β^- and β^+ spectra. The theoretical $B(GT^-)$ strengths vs E_m are shown in Fig. 2. The

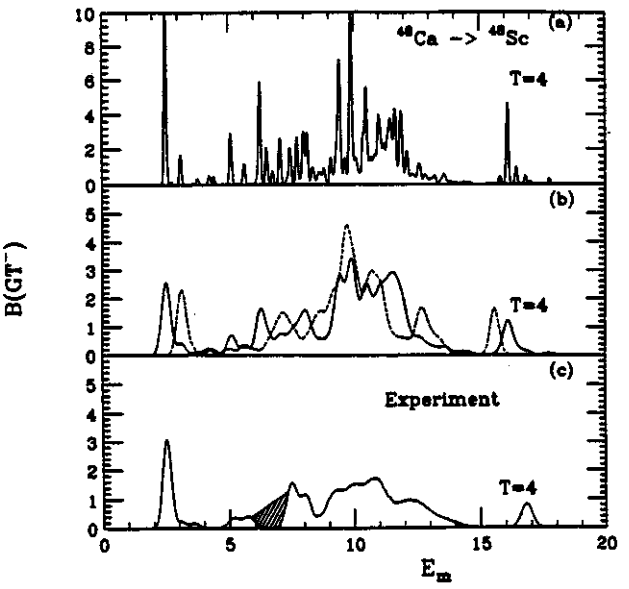

Fig. 2 The $B(GT^-)$ spectra for $^{48}Ca \rightarrow ^{48}Sc$. The high resolution spectrum (100 keV) obtained with the MSOBEP interaction is shown in 2(a). The low resolution spectra (400 keV) obtained with the MSOBEP (solidline) and MH interaction (dashed line) are shown in 2(b). The effective operator defined in Eq. (2) is employed in our calculations. The experimental $B(GT^-)$ from Ref. 28 and B.D. Anderson (Private communication) is presented in 2(c). The hatched area indicates the uncertainty resulting from subtracting the Fermi strength in the 0^+ (T=4) state at 6.8 MeV.

experimental distribution in Fig. 2(c) represents the strength above the background line in Fig. 1 of Ref. 23. There is additional strength in the background between 4.5 and 14.5 MeV not shown in Fig. 2(c) but indicated in the numerical comparisons made in Table 1. There may be more strength in the background above 14.5 MeV which we will comment on later. The experimental spectrum in Fig. 2(c) was obtained by the fitting the experimental cross section to a series of Gaussian peaks and then converting the cross section in each peak into a Gamow-Teller strength (Ref. 23 and B.D. Anderson, private communication). Because the experimental measurement has a finite resolution, the theoretical $B(GT^-)$ spectra are smoothed by a Gaussian. The $B(GT^-)$ spectrum with a resolution (FWHM=100 keV) is shown in Fig. 2(a) for the MSOBEP interaction. The low resolution spectra for the MSOBEP (solid line) and MH (dashed line)

interactions shown in Fig. 2(b) was obtained with FWHM=400 keV. One normalized factor is introduced in Fig. 2 to make the areas proportional to the $B(GT^-)$ strength. The $B(GT^-)$ values extracted from the (p,n) data are compared with the theory in Table 1. For the broad peak between 4.5 - 14.5 MeV, the minimum experimental value of 8.61 corresponds to the spectrum in Fig. 2(c). An additional amount of 2.86 was estimated to be in the background not shown in Fig.2(c).[23]

Table 1. Summary of the $B(GT^-)$ and $B(GT^+)$ values obtained from experiments and compared to the theoretical calculations with the MSOBEP and the MH interactions.

	E_m (MeV)	Experiment[a]	MSOBEP	MH
	2.52-3.5	1.30	1.32	1.24
β^-	3.5-14.5	8.61+2.86[b]	12.31	12.39
	16.8(T=4)	0.45	0.42(0.62)[c]	0.72(0.73)[c]
	2.52	0.07	0.07	0.15
β^+	3.0-6.0	0.49	0.50	0.51
	>6.0	?	0.03	0.10

a. The experimental $B(GT^-)$ and $B(GT^+)$ strengths from Refs. 28 and 29.
b. The B(GT) in the experimental background in the region of $4.5 \leq E_m \leq 14.5$ MeV.[28]
c. The first number is the strength in the single strongest T=4 state whereas the number in the bracket includes the additional strength from small states ±500 keV on either side of the strongest state.

The theoretical and experimental shapes are qualitatively the same as well as the $B(GT^-)$ strength values themselves (see Table 1). But quantitatively there are some interesting differences which indicate a preference for the MSOBEP over the MH interaction. In the pure j-j coupling model, the first 1^+ excited state in ^{48}Sc can be understood as a $(\pi f_{7/2} \nu f_{7/2}^{-1})$ particle-hole configuration. The theoretical calculation based on the MSOBEP interaction and the experimental data are both in good agreement with this simple picture. But for the MH interaction, this particle-hole state is the second 1^+ excited state located at 3.13 MeV. The first 1^+ of ^{48}Sc in the MH calculation has a negligibly small $B(GT^-)$ value. This state, however, has a relatively large overlap with ^{46}Ca plus a deuteron-cluster configuration, which explains why the state comes low in energy.

The total $B(GT^-)$ strengths in T=4 states are 0.78 and 0.77 for the MSOBEP and MH interactions, respectively. For the MSOBEP interaction, only $B(GT^-)$=0.42 contributes to the single state at 16.1 MeV, the rest is spread between 15 - 20 MeV (see Fig. 2a.) But for the MH interaction, most of the $B(GT^-)$ strength (0.72) is in a single state at 15.4 MeV. Thus comparison with experiment again favors the MSOBEP interaction (see Table 1).

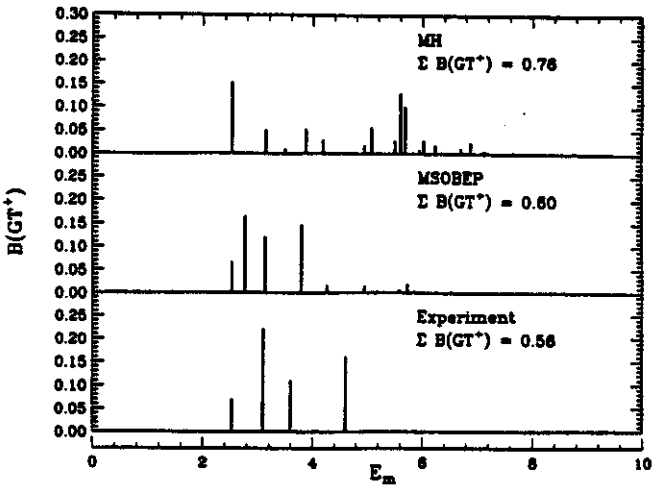

Fig. 3 The $B(GT^+)$ values for $^{48}Ti \rightarrow {}^{48}Sc$. The experimental values from Ref. 29 and compared to the results obtained with the MSOBEP and MH interactions. The effective operator defined in Eq. (2) is employed in our calculations.

The β^+ strength distribution and total strengths for theory and experiment[24] are compared in Fig. 3 and in Table 1. There is the possibility for $B(GT^+)$ strength above 6 MeV in the data[24] not shown in Fig. 3. We see that the β^+ spectrum and $\Sigma B(GT^+)$ are strongly dependent on the effective interactions. The spectrum for the MSOBEP interaction is in best agreement with the experiment, especially for the first state (see Table 1).

Calculated $M_{GT}^{2\nu}$ values are presented in Table 2 and compared with previous calculations.

Table 2. Comparison of the nuclear matrix elements B(cls) and $M^{2\nu}_{GT}$, the average excited energy $\langle E_m \rangle$ and half life $T_{1/2}$. The shell-model space configurations are described by $f^{8-n}_{7/2}(p_{3/2}f_{5/2}p_{1/2})^n$ with n=0 to n_{max} for the fp shell referring to the initial (i), intermediate (m) and final (f) states.

Reference	Interaction	n_{max} i	m	f	B(cls)	$M^{2\nu}_{GT}$ $(MeV)^{-1}$	$\langle E_m \rangle$ (MeV)	$T_{1/2}$ $(10^{19}yr)$
Experiment[27]								>3.6
present	MSOBEP	4	5	4	0.204	0.070	1.06	1.9
present	MH	4	5	4	0.213	0.055	2.01	3.0
Ref. 9[a]	MH	8	8	8		0.053		3.3
Ref. 1[a]	KB[1]	8		4	0.266			7.2[b](1.1[c])
Ref. 4[a]	MH	2	2	2	0.278	0.073	1.94	1.7
Ref. 8[a]	MBZ[8]	0		0	0.216			
Ref. 6[a]	KB[17]	0		0	0.150			

a. Modified by taking into account the effective operator in Eq. (2).
b. Based on an assumed $\langle E_m \rangle$ = 5.86 MeV.
c. Based on the exact $\langle E_m \rangle$ = 1.06 MeV.

We have modified the results from previous calculation to take into account the effective operator of Eq. (2). We note that the value of $\langle E_m \rangle$=5.86 MeV assumed by Haxton is too large in agreement with the conclusion of Ref. 4. We also note the excellent agreement between our result with the MH interaction and the result obtained with the new method of Ogawa and Horie[6] who also used the MH interaction. This new method implicitly takes into account the spectrum of intermediate states exactly in the full basis. But it does not produce the explicit intermediate state spectrum which was important for the β^- and β^+ comparisons made above.

Beyond the fp shell model space there are several processes which we should consider. The role of Δ-isobar admixtures have been investigated in previous work.[16,17,19,20] The contribution from the direct excitation of the Δ-isobar nucleon-hole configuration, for which the excitation energy is about 300 MeV, is negligible because of the cancellation between β^+ and β^- and because of the large energy denominator in Eq. (3). The Δ-isobar admixtures in the low-lying states are already approximately taken into account in our calculation in the effective operator $\bar{\sigma}t$ of Eq. (2) as well as in the effective interaction. In addition, 2p2h admixtures beyond the fp shell can lead to B(GT) strength at higher excitation.[18] The possible strength seen experimentally in the background above 6 MeV in β^+ and 15 MeV in β^- may be due to these 2p2h admixtures. The effect of these 2p2h admixtures are also approximately taken account in the effective operator and effective interaction. The contribution from the direct excitation of the 2p2h configurations may again be small because of cancellation and large energy denominator but should be investigated further.

With the MSOBEP interaction we predict the $2\nu\beta\beta$ decay matrix element of ^{48}Ca is $M^{2\nu}_{GT}$ =0.070 giving a half life $T_{1/2}$= 1.9 × 10^{19}yr, which differs by nearly a factor of two from the experimental limit[22] of $T_{1/2} > 3.6 \times 10^{19}$ yr. We note that the $T_{1/2}$ obtained with the MSOBEP and MH interactions are not very different, indicating the relative stability of the calculation with respect to reasonable

variations in the interaction. These comparisons suggest that it would be important to confirm and improve upon the experimental limit. As a next step, we plan to use the wave functions of ^{48}Ca and ^{48}Ti based on the MSOBEP interaction to calculate the $0\nu\beta\beta$ decay matrix elements.

---

[a]Physics Department, University of Stellenbosch, Stellenbosch, South Africa

References

1. W.C. Haxton and G.J. Stephenson, Prog. Part. Nucl. Phys. 12,409(1984).
2. Doi, T. Kotani and E. Takasugi, Prog. Theor. Phys. suppl. 83,1(1985).
3. K. Muto and H.V. Klapdor, Neutrinos, Editor H.V. Klapdor, Springer-Verlag, in press.
4. T.Tsuboi, K. Muto and H. Horie, Phys. Lett. 143B,293(1984).
5. L. Zamick and N. Auerbach, Phys. Rev. C26}, 2185(1982).
6. K. Ogawa and H.Horie, Nuclear Weak Process and Nuclear Structure, (World Scientific) p. 308.
7. K. Grotz and H.V. Klapdor, Nucl. Phys. A460,395(1986).
8. A. Etchegoyen, W.D.M. Rae, N.S. Godwin, W.A. Richter, C.H. Zimmerman, B.A. Brown, W.E. Ormand and J.S. Winfield, MSU-NSCL report #524 (1985).
9. K. Muto and H. Horie, Phys. Lett. 138B,9 (1984).
10. W.A. Richter, R.E. Julies and B.A. Brown, unpublished.
11. J.B. McGrory, B.H. Wildenthal and E.C. Halbert, Phys. Rev. C2,186(1970).
12. T.T.S. Kuo and G.E. Brown Nucl. Phys. A114,241(1968)
13. J.B. McGrory, and B.H. Wildenthal Phys. Lett. 103B,173(1981).
14. B.A. Brown, W.A. Richter, R.E. Julies and B.H. Wildenthal, Ann. Phys. 182,191(1988).
15. B.A. Brown and B.H. Wildenthal, Ann. Rev. of Nucl. Part. Sci. 38,29(1988).
16. C.D. Goodman, et. al. Phys. Lett. 107B,406 (1981).
17. A. Bohr and B.R. Mottelson, Phys. Lett. 100B,10(1981)
18. G.F. Bertsch and I. Hamamoto Phys. Rev. C26,1323(1982).
19. A. Arima, K. Shimizu, W. Bentz and H. Hyuga Adv. Nucl. Phys. 18,1(1987).
20. I.S. Towner Phys. Rep. 155 No. 5 (Nov. 1987).
21. A.H. Wapstra and G. Audi, Nucl. Phys. A432, 1(1985).
22. R.K. Bardin, et. al., Nucl. Phys. A158,337 (1970).
23. B.D. Anderson, et. al. Phys. Rev. C31,1161 (1985).
24. W.P. Alford, et. al. Preprint, Gamow-Teller Strength Observed in the $^{48}Ti(n,p)^{48}Sc$ Reaction. Implication for the Double Beta Decay of ^{48}Ca

Table 1. Summary of the $B(GT^-)$ and $B(GT^+)$ values obtained from experiments and compared to the theoretical calculations with the MSOBEP and the MH interactions.

	E_m (MeV)	Experiment[a]	MSOBEP	MH
	2.52-3.5	1.30	1.32	1.24
β^-	3.5-14.5	8.61+2.86[b]	12.31	12.39
	16.8(T=4)	0.45	0.42(0.62)[c]	0.72(0.73)[c]
	2.52	0.07	0.07	0.15
β^+	3.0-6.0	0.49	0.50	0.51
	>6.0	?	0.03	0.10

a. The experimental $B(GT^-)$ and $B(GT^+)$ strengths from Refs. 28 and 29.
b. The B(GT) in the experimental background in the region of $4.5 \leq E_m \leq 14.5$ MeV.[28]
c. The first number is the strength in the single strongest T=4 state whereas the number in the bracket includes the additional strength from small states ±500 keV on either side of the strongest state.

AN RPA PROGRAM

George F. Bertsch

The random phase approximation to collective excitations of Fermi systems is one of the most important tools of theoretical spectroscopy, but there exist few readily available programs. To remedy this we have written a "bare-bones" program, RPA3, that is easy to use and is also well documented. RPA3 program may be obtained by electronic mail from Bertsch@MSUNSCL.

The program uses the response function method following Ref. 1. This allows essentially complete configuration spaces to be treated, and effects of the continuum are automatically included. Energy-weighted sum rules are satisfied to a numerical accuracy of a few percent. The disadvantage of the method is that interactions must be local; in fact in the program there is a further restriction to density-dependent delta-function interactions.

In principle, the RPA is based on a self-consistent mean field description of the ground state. Rather than requiring user input of the self-consistent wave functions or including a subprogram to do this, RPA3 constructs a model ground state using a Woods-Saxon potential.

The input to the program consists of mesh parameters, A and Z of the nucleus, quantum numbers of occupied orbits, parameters of the residual interaction in Skyrme form, multipolarity of the response, and energy range to be studied.

The output of the program is the response function

$$S(\omega) = \sum_f \langle i|M|f\rangle^2 \delta(E_f - E_i - \omega)$$

or the smoothed response function $S_r(\omega) = \int dE \frac{S(E)}{2\pi} \frac{r}{(E-\omega)^2+(r/2)^2}$. Here the operator M is either a multipole operator or some operator defined by the user.

Some sample results are shown in Figs. 1-3.

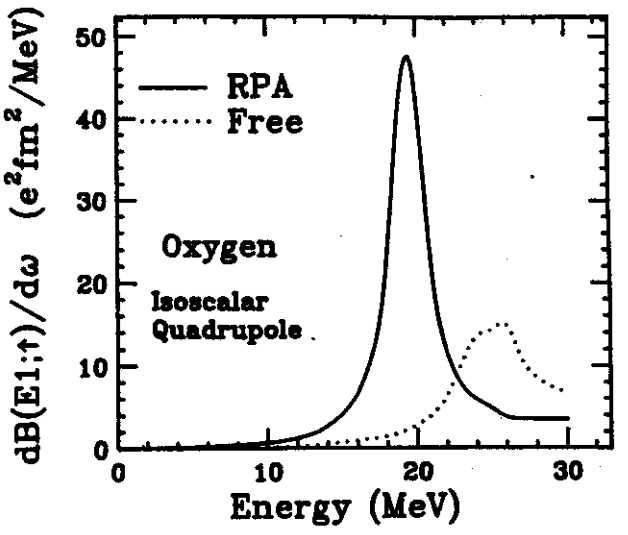

Fig. 1 Isoscalar quadrupole response in ^{16}O. The dashed line is the free response (no residual interaction) and the solid line is the RPA response. The residual interaction is of the Skyrme form with t_0=-1100 MeV-fm^3, t_3=15,000 MeV-fm^5 and x=0.5.

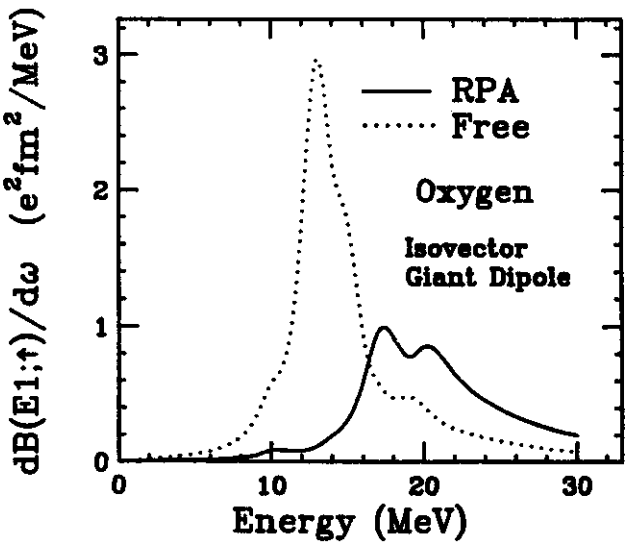

Fig. 2 Isovector dipole response in ^{16}O. Dashed and solid lines are free and RPA responses, respectively, computed with r=1 MeV. Note that the residual interaction shifts the strength upward, but not enough to reproduce the empirical giant dipole energy, 23.5 MeV.

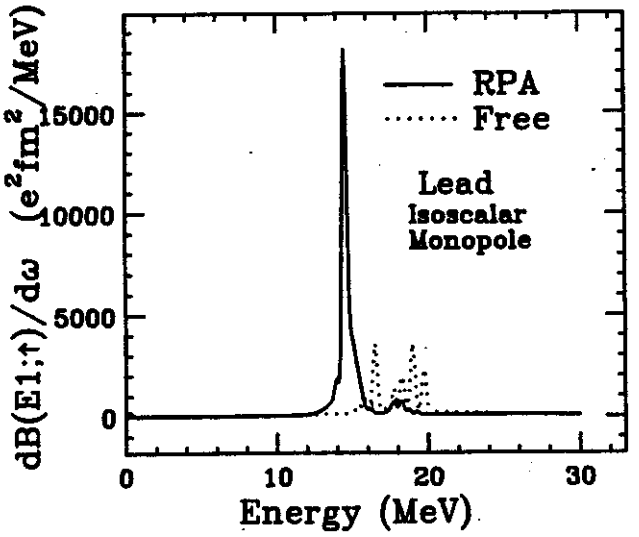

Fig. 3 Monopole response in ^{208}Pb. Parameters are the same as in Figs. 1 and 2.

References

1. S. Shlomo and G. Bertsch, Nucl. Phys. A243, 507(1975).